dRTI: Directional Radio Tomographic Imaging

Bo Wei[†‡∀], Ambuj Varshney[§], Neal Patwari[⌀△],
Wen Hu[†‡∀], Thiemo Voigt[∀§], Chun Tung Chou[†]
[†] University of New South Wales, Sydney, Australia [∀] SICS, Stockholm, Sweden
[‡] CSIRO, Brisbane, Australia [§] Uppsala University, Uppsala, Sweden
[⌀] University of Utah, Salt Lake City, USA [△] Xandem Technology, Salt Lake City, USA
{bwei,wenh,ctchou}@cse.unsw.edu.au[†], ambuj.varshney@it.uu.se[§],
npatwari@ece.utah.edu[⌀], thiemo@sics.se[∀]

ABSTRACT

Radio tomographic imaging (RTI) enables *device free* localisation of people and objects in many challenging environments and situations. Its basic principle is to detect the changes in the statistics of radio signals due to the radio link obstruction by people or objects. However, the localisation accuracy of RTI suffers from complicated multipath propagation behaviours in radio links. We propose to use inexpensive and energy efficient electronically switched directional (ESD) antennas to improve the quality of radio link behaviour observations, and therefore, the localisation accuracy of RTI. We implement a directional RTI (dRTI) system to understand how directional antennas can be used to improve RTI localisation accuracy. We also study the impact of the choice of antenna directions on the localisation accuracy of dRTI and propose methods to effectively choose informative antenna directions to improve localisation accuracy while reducing overhead. Furthermore, we analyse radio link obstruction performance in both theory and simulation, as well as *false positives* and *false negatives* of the obstruction measurements to show the superiority of the directional communication for RTI. We evaluate the performance of dRTI in diverse indoor environments and show that dRTI significantly outperforms the existing RTI localisation methods based on omni-directional antennas.

1. INTRODUCTION

This paper explores the use of directional antennas to improve the accuracy of radio tomographic imaging (RTI). RTI uses a network of small inexpensive wireless devices, placed in the periphery of an Area of Interest (AoI), to estimate the locations of people and objects within the AoI [25, 26]. A distinguishing feature of RTI is that it is *device free* [32] in the sense that the people and objects to be tracked do not have to wear any special purpose devices on them. This makes RTI significantly less intrusive compared with many other localisation methods which require people/objects to carry a radio device or tag. In addition, RTI can function in many challenging environments. RTI can work in both line-of-sight (LOS) and non-LOS (NLOS) environments. RTI can work with no or poor lighting conditions because it uses radio waves rather than visible light. The wireless devices for RTI can be placed outside the walls to enable them to *see through walls* or smoke to locate people or objects within the walls. Therefore, *RTI has a broad range of applications in emergency response, security (e.g. hostage rescue), health care, and assisted living etc.* [4, 9].

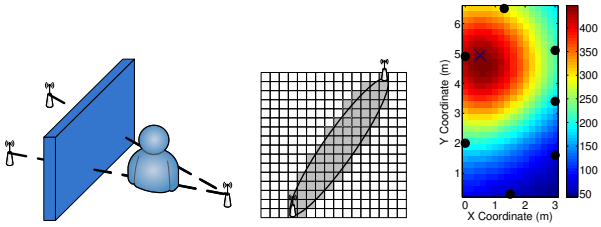

Figure 1: (a) A person blocks two radio links, creating a NLOS environment. (b) The AoI is divided into voxels. An ellipse is used to model the area of obstruction between a pair of nodes. (c) An example of an RTI image. The blue cross indicates the truth location of the obstruction. (Best view in colour.)

The key idea behind RTI is that people/objects in the AoI present themselves as *obstructions* to radio waves. For example, in Fig. 1(a), a person stands in the paths of two radio links, and her presence can be detected by observing the *changes* of some statistics of the radio links.

Previous work on RTI relies on omni-directional antennas, which radiate power isotropically in the horizontal plane. Multipath radio channels experience *multipath fading*, in which arriving waves unpredictably experience constructive or destructive interference. Directional antennas reduce the spatial extent of significant multipath, and thus the effects of fading, by focusing the radiated power in some given directions. The benefits of RTI with directional antennas (dRTI) are twofold compared to their omni-directional counterparts. First, the presence of obstructions which block the direct paths will have significantly more impact on the link quality when links use directional antennas. Second, the presence of obstructions which are *outside* the direct paths will have significantly less impact on the link quality of directional antennas. Therefore, directional antennas can provide significantly better link obstruction observations to improve the

RTI localisation accuracy. A conspicuous change in these radio link quality statistics will result in better location estimate, as well as reduce the number of false positives and negatives.

Directional antennas have been explored to improve the communication performance on mobile phones and wireless networks previously [3, 12]. However, traditional directional antennas such as Yagi antennas have a large form factor and consume a large amount of energy to move from one direction to another direction, which makes them unsuitable for resource-impoverished Wireless Sensor Networks (WSNs) with small nodes. On the other hand, Electronically-Switched Directional (ESD) antennas [17] are significantly more energy efficient compared to tranditional directional antennas, and enable *dynamic* electronic control of direction of maximum gain. Recently, Mottola et al. [14] leveraged ESD antennas to alleviate wireless contention in WSNs. In this paper, we, for the first time, explore the use of ESD antennas to improve RTI localisation accuracy. We detail the feasibility studies for an inexpensive and energy efficient dRTI WSN system with ESD antennas and answer the fundamental questions whether and to what extent dRTI systems can improve tracking performance in practice.

Although dRTI can significantly improve localisation accuracy, its overhead due to the use of directional antenna is high. Consider a transmitter and receiver, each equipped with a directional antenna that can point in n different directions. The total number of antenna direction pairs is n^2. Hence, conducting link quality measurements on all the possible antenna direction pairs results in higher communication overhead and energy consumption. Moreover, not all n^2 antenna direction pairs are useful for RTI localisation estimation. We therefore investigate three different methods to select antenna direction pairs to reduce overhead while maintaining accurate position estimation. The contributions of this paper are as follows:

1) We conduct comprehensive investigations to demonstrate that directional antennas can produce sharper changes in radio link quality statistics (both mean and variance) compared to their omni-directional counterparts.

2) We analyse radio link obstruction performance in both theory and simulation, and *false positives* and *false negatives* of the obstruction measurements to provide an insight on the superiority of the directional communications for RTI.

3) We carry out studies to understand how the choice of directional antenna pairs can impact on the radio link quality statistics. Based on these studies, we propose three methods to choose the informative directional antenna pairs to increase the accuracy of RTI while reducing the overhead of the system.

4) We design and implement dRTI, the first system that improves indoor tracking accuracy through the use of ESD antennas, and evaluate the performance of the proposed dRTI system in realistic LOS and NLOS environments. Our results show that the proposed dRTI system can improve the localisation accuracy significantly compared to state-of-the-art RTI system based on the mean of link quality (mRTI) [25], the variance of link quality (vRTI) [26] and multi-channel RTI (cRTI) [8] using omni-directional antennas.

The rest of this paper is organised as follows. Section 2 presents background on RTI and ESD antennas. Section 3 presents a few different studies: (1) The impact of obstructions on the link quality statistics for both directional and omni-directional antennas; (2) The variation of link quality statistics for different choices of directional antenna pairs. Based on these studies, we propose three different methods to choose effective directional antenna pairs to reduce overhead in dRTI. We present comprehensive evaluations of our dRTI system and show the statistics of the radio link obstruction measurement *false positives* and *false negatives* in Section 4. Related work is presented in Section 5. Finally, we conclude the paper in Section 6.

2. BACKGROUND

The mathematical notations used in this paper are summarised in Table 1.

Table 1: Mathematical Notations

Symbol	Description
M	Number of links in the network
N	Number of voxels in the AoI
$R_i(t)$	RSS measurement for link i at time t (omni only)
$\bar{R}_i$	Mean RSS measurement for link i during calibration (omni only)
$y_i(t)$	link quality statistics for link i at time t
y	a $M \times 1$ vector of link quality statistics
x	a $N \times 1$ vector of tomographic image
F_i	The set of selected *Pattern Pair*s for link i
$R_{i,j}(t)$	RSS measurement for link i, *Pattern Pair* j at time t (dRTI only)
$\bar{R}_{i,j}$	Mean RSS measurement for link i, *Pattern Pair* j during calibration (dRTI only)

2.1 Radio Tomographic Imaging

The aim of RTI is to localise the people and objects (Note: we will also use obstructions to refer to people or objects because this is how RTI "sees" them.) within an AoI by using sensors placed around the periphery of the AoI. We assume that the AoI is divided into voxels, see Fig. 1(b). The sensors exchange packets periodically in order to monitor the Received Signal Strength (RSS) of the links over time. In RTI, all links are assumed to be *asymmetric*.

RTI localises the obstructions in the AoI in two steps. A *tomographic image* is first computed from the RSS measurements, and then a Kalman filter is used to track the obstructions from the computed image.

We use the RTI model introduced in [25] to compute the tomographic image. This model is also used in many other RTI works [8, 9, 13, 26, 33]. Let $R_i(t)$ denote the RSS measurement of the i-th link at time t. We use $R_i(t)$ to compute some link quality statistics $y_i(t)$ for link i. These link statistics $y_i(t)$ will be used to compute the tomographic image later on. We consider the following link quality statistics in this paper.

Mean based RTI (mRTI): The *original* mRTI method is proposed in [25] where RTI is used in an *open* outdoor environment. This is a fairly simple radio environment where radio signal obstruction is due mainly to LOS path loss. The effect of an obstruction in a radio link is to decrease the RSS values of that link. Therefore, one may detect the presence of an obstruction in the link i at time t by testing whether $R_i(t)$ has decreased from a base value. The mRTI method requires a calibration period where obstructions are absent in the AoI. During this period, the sensors exchange packets in order to determine the mean RSS of each link. Let $\bar{R}_i$

be the mean RSS of link i over the calibration period. The original mRTI uses the link statistics $y_i(t) = R_i(t) - \bar{R}_i$ for link i.

We will be concerned with RTI in an indoor environment in this paper. We will see later on that, in the indoor environment, the presence of an obstruction in a radio link can cause the RSS of the link to decrease, increase or stay at the same value. The original mRTI therefore does not work well. In this paper, we use mRTI to mean the *modified* link statistics $y_i(t) = |R_i(t) - \bar{R}_i|$ where absolute value is used because the RSS can increase or decrease.

Variance based RTI (vRTI): The vRTI [26] method uses the variance of a window of v measurements as the link quality statistics, i.e. $y_i(t) = var(R_i(t), ..., R_i(t - v + 1))$. Since this method does not require a base value, no calibrations are required.

We collect the $y_i(t)$ for all the M links in the WSN to form the link quality statistics vector y. We use y to estimate the tomographic image x which is a $N \times 1$ vector where N is the number of voxels in the AoI. Each element of x corresponds to a voxel. If the i-th element of x has a larger value, then the chance of the obstruction is in the i-th voxel is higher. Fig. 1(c) shows an example tomographic image as an heat map (best view in colour). It can be seen that the true location of the obstruction, which is marked by a cross, is in an "hot" area. To obtain x from y, the RTI model in [25] assumes that y and x are linearly related $y = Ax + n$, where n is a noise vector and A is a $M \times N$ matrix. The (i, j) element of A is given by [25, 26]:

$$A_{ij} = \frac{1}{\sqrt{d}} \begin{cases} 1 & \text{if } d_{ij}(1) + d_{ij}(2) < d + \lambda \\ 0 & \text{otherwise} \end{cases}, \qquad (1)$$

where d is the distance between the nodes of link i, $d_{ij}(1)$ and $d_{ij}(2)$ are the distances from the voxel j to the two nodes of link i, and λ is a parameter to tune the width of the ellipse. If A_{ij} is non-zero, then it means voxel j is close to the line connecting the nodes of link i and is likely to contribute to the variation that is found in the link quality statistics $y_i(t)$. The non-zero elements of A_{ij} for a given link i form an ellipse, see Fig. 1(b) where the shaded voxels indicates those A_{ij} that are non-zero for the link consisting of the two nodes shown in the figure.

Since the number of voxels N is normally greater than the number of links M, Eq. (**??**) is under-determined and can be solved by using Tikhonov regularization [25]. The estimated maximum of the tomographic image is then input into a Kalman filter for location estimation and tracking. The details can be found in [25, 26].

2.2 Electronically Switched Directional Antenna

ESD antennas are able to electronically control the direction of the maximum antenna gain, which is feasible for the resource constrained WSNs as demonstrated earlier [7, 17]. Nilsson [17] has designed an ESD antenna based on the concept of Electrically-Steerable Parasitic Array Radiator (ESPAR). ESPAR antennas consist of a central monopole surrounded by a number of parasitic elements. In the simplest form, the parasitic elements can be either grounded or isolated allowing them to act as reflectors when grounded and as directors when isolated.

In this paper, we use ESPAR antennas, each of which has six parasitic elements designed by Nilsson [17]. The parasitic elements can be individually grounded or isolated via software APIs. When all the parasitic elements are grounded except one, the direction of the maximum antenna gain is towards the direction of the isolated element. We use this configuration for the dRTI experiments. When all the parasitic elements are isolated, we have an omni-directional configuration of the antenna. We use this configuration for omni RTI and cRTI experiments. Measurements in [17] show the ESD antenna directional dB gain patterns fit a sinusoidal model, $g_{dB}(\theta) = -1.565 + 5.835cos(\theta - \theta_0)$ where θ_0 is the pointing direction.

3. RADIO TOMOGRAPHIC IMAGING WITH DIRECTIONAL COMMUNICATIONS

In order to motivate future sections, Fig. 2 compares the localisation error between omni-directional RTI and dRTI. These experiments are conducted within 10 ms of each other so their channel conditions can be assumed to be *comparable*. The RTI image for omni in Fig. 2(b) shows a larger error compared to that of dRTI in Fig. 2(d). In order to explain this difference, we look at the vRTI link quality statistics, which are indicated by the thickness of the lines connecting the node pairs, in Fig. 2(a) and Fig. 2(c) for omni and directional. Fig. 2(a) shows that a deep fade between Nodes 2 and 5 has led omni-vRTI to believe that an obstruction is likely to be present between these two nodes, as shown by the high value of tomographic image for the voxels around the line joining these nodes. However, this deep fade had little impact on dRTI. Our hypothesis is that *directional communication is sensitive to obstruction over a large range of orientations. This results in both larger changes in RSS and larger RSS variance. Moreover, these changes are less affected by fading.* We will provide empirical evidence to support this hypothesis next.

3.1 The Impact of Directional Communications on RSS Changes and Variance

This section presents empirical evidence that directional antenna links, when obstructed, produce larger changes in RSS and larger RSS variance in most antenna directions.

3.1.1 Experimental Setup

We employ two TelosB nodes running the Contiki operating system. Each node has an ESD antenna with 6 parasitic elements equally spaced at 60° apart. The nodes can *dynamically* change the sending direction to one of the six directions or send omni-directionally by setting a digital output pin. It takes less than 1 ms to change the sending direction. The RSS Indicator (RSSI) values are read from the TI CC2420 transceivers and converted to RSS values in dBm according to the transceiver datasheet.

We conduct experiments in both indoor LOS and NLOS ("through-wall") environments in our lab. We only report the results of the NLOS experiment here because we observe similar results for the LOS environment. For the NLOS environment, we place the two nodes, approximately 3 meters apart, in two different rooms. The wall between the rooms is made of glass and wood. We label the antenna directions with a number from 1 to 6. The *Direction 1*s of the two nodes face each other (shown in Fig. 3). A person walks through the link of the two nodes *multiple times* to block it.

The transmitter sends small packets to the receiver in each of the six directions, as well as omni-direction as fast as possible, and the receiver receives the packets from all six directions and omni-direction. The transmission node

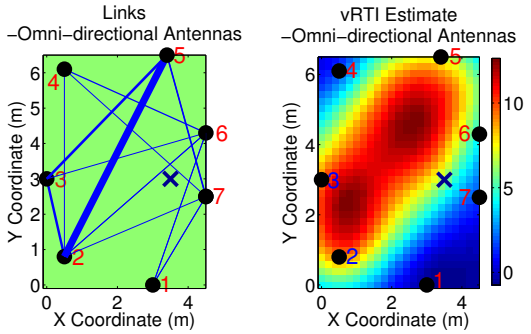

(a) RTI with omni-directional antennas.

(b) The produced image from (a) (Picture view best in colour).

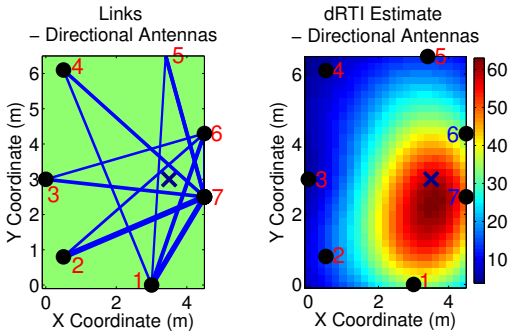

(c) RTI with *directional* antennas.

(d) The produced image from (c) (Picture view best in colour).

Figure 2: Omni-directional RTI vs dRTI. The thicknesses of lines in (a) and (c) are proportional to the vRTI link quality statistics. The crosses (×) show the true location of the obstruction. Fig. (b) shows that the RTI image with a large localisation error because of a deep fade between Nodes 2 and 5 in (a). However, this fade has little impact on dRTI estimation shown in (d).

ID, direction, and the sequence number are included in the packets. When the receiver receives a packet, it appends the receive direction and RSSI value into the packet as well. Therefore, we can figure out the transmit direction, receive direction and RSS value of each received packet. For a radio link from a transmitter to a receiver, there are $6 \times 6 = 36$ possible *transmit-receive antenna direction pairs* and we will refer to them as *Pattern Pairs*. Furthermore, there are two links (uplink and downlink) between two nodes.

3.1.2 The Impact to RSS Changes and Variance

Fig. 4(a) shows the RSS measurements of one of the *Pattern Pairs* and omni when a person attenuates the radio signal between time 50 and 55. It is clear that the *Pattern Pair* has a significantly bigger change in RSS measurement than omni. We compute the mRTI and vRTI of the RSS measurements for the 36 *Pattern Pairs* and omni. (Note that mRTI and vRTI in Section 2.1 are defined for a link. We simply consider a *Pattern Pair* as a link in the calculation.) We compare the average mRTI and vRTI over the 36 *Pattern Pairs* against that of omni in Fig. 4(b) and 4(c). These figures show that both the change in RSS and variance of RSS are bigger for directional antennas. In particular, the average RSS variance over all 36 *Pattern Pairs* is almost twice that of omni. This experiment demonstrates that *directional communications are indeed more sensitive to the obstruction, and produce larger changes in RSS and larger changes in RSS variance.* Fig. 4(b) and 4(c) also show the standard deviation of the mRTI and vRTI over the 36 *Pattern Pairs*. The standard deviation is of almost the same magnitude as the average. We will discuss the variation of mRTI and vRTI among the *Pattern Pairs* later.

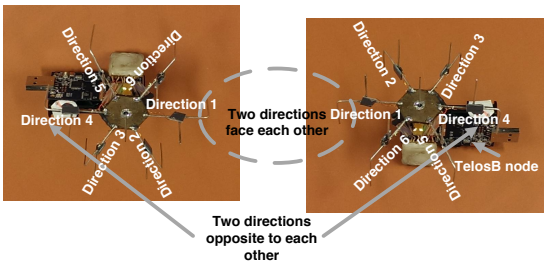

Figure 3: The physical ESD antenna directions of two nodes. TelosB node is marked in the figure.

3.1.3 Theoretical Analysis on Radio Link Obstruction Performance

Simple propagation models can be used to quantify the impact of antenna directionality on the spatial area in which a person's movements will cause a link to experience high RSS variance. We call this area the "spatial impact area". By assuming a homogeneous Poisson field of reflectors, a cylinder model for a human body, and a standard path loss exponent received power model allows one to analytically calculate a value (Expected Total Affected Power, or ETAP) which is proportional to the variance experienced by a link as a function of a person's coordinate [19]. Here, we extend the analysis to include directional antennas. We use the ESD antenna gain function $g_{dB}(\theta)$ given in Section 2.2. We modify Eq. (19) from [19] to include the product of the (linear) transmitter and receiver antenna gains in the received power equation, and numerically integrate to find the ETAP [1]. The results, for the same parameters used in [19], are shown in Fig. 5(a), for the case when the directions of the *Pattern Pair* on the two nodes are pointed directly at each other, which can be directly compared to Fig. 5(b) which shows the result for omnidirectional antennas[2]. The results show that the spatial impact of a person in between the two nodes is dramatically reduced; the -15 dB contour lines with omni antennas are about 150% of the path length apart at the center of the link line; with directional antennas the same width measurement is 75% of the path length. We note that there is almost no variance expected when the person is behind either node (i.e., with x-coordinate < -1 or > 1). Interestingly, the -3 and -6 dB contour lines are almost unaffected; it is specifically the low-variance impact areas that are dramatically narrowed. This helps RTI reduce radio link

[1]More details are available in [19] and the technical report of this paper.

[2]We focus on the impact of reflection here because scattering (the other impact studied in [19]) is less important as the power in scattered waves are generally lower [19]. Furthermore, for scattered waves, the ESD antenna has a similar effect and is omitted for brevity.

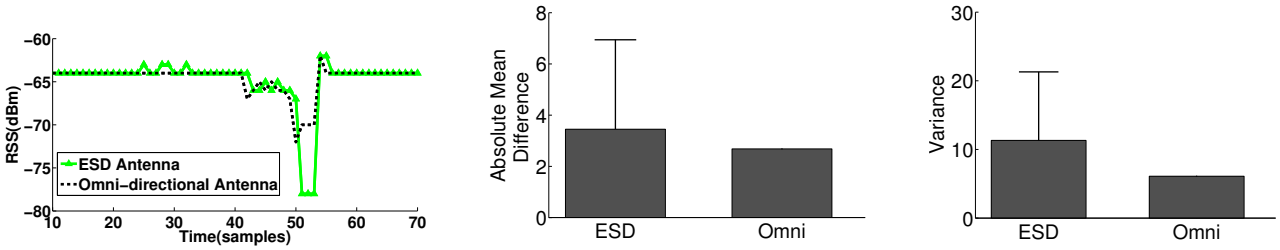

(a) RSS measurement change (b) mRTI (c) vRTI

Figure 4: (a) RSS measurement of a selected *Pattern Pair* and the omni-directional antenna. (b) The average mRTI over 36 *Pattern Pairs* versus mRTI of omni. (c) The average vRTI over 36 *Pattern Pairs* versus vRTI of omni. The error bars indicate one standard deviation.

obstruction *False Negatives* and *False Positives*, which will be discussed in next section.

The simulation results of ETAP using ESD antennas, for the same method and parameters used in [19], are shown in Fig. 6(a). We performed 100 trials and the average affected power for a given human location is calculated as our estimate of ETAP. The simulation results match those of the analytical results shown in Fig. 5 closely.

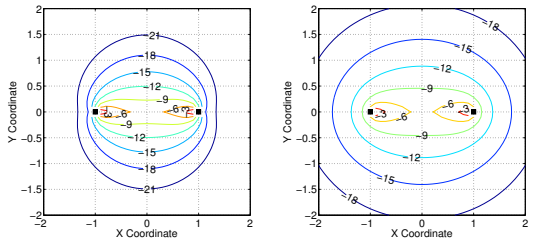

(a) ESD antennas "at each other" (b) Omni-directional antennas

Figure 5: Analytical "spatial impact area": ETAP (which is proportional to expected value of the RSS variance), in dB relative to the maximum, as a function of person position, with transmitter and receiver (■) at (-1, 0) and (1, 0), respectively.

3.1.4 *Radio Link Obstruction False Negatives and False Positives*

We say that a radio link obstruction *false negative (FN)* has occurred if the RSS measurements remain stable (i.e., with little change and small variance) in the presence of an obstruction in the LOS path (e.g., within the shaded area in Fig. 1(b)). Similarly, we say that a radio link obstruction *false positive (FP)* has occurred if the link quality RSS measurements change significantly when no obstructions are present in the LOS path. Both *FN* and *FP* frequently occur in RTI systems, especially in the NLOS cluttered environments. These errors can significantly impact on the accuracy of RTI localisation.

A benefit of directional antennas is that they can reduce the instances of *FP* and *FN*. The model in Section 3.1.3 shows that the directional antennas reduce the spatial area size by the impact of a person significantly compared to omni direction ones (see Fig. 5 and 6), which helps to reduce the instances of *FP*. Furthermore, they focus on their radio

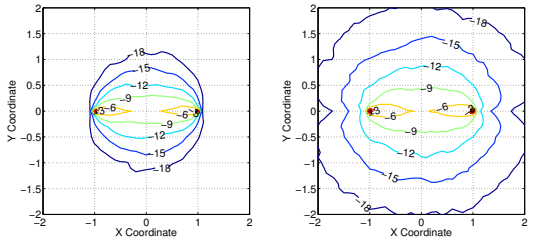

(a) ESD antennas "at each other" (b) Omni-directional antennas

Figure 6: Simulated "spatial impact area": ETAP (which is proportional to expected value of the RSS variance), in dB relative to the maximum, as a function of person position, with transmitter and receiver (■) at (-1, 0) and (1, 0), respectively.

emission energy at the direct path direction, which helps to reduce the instances of *FN*. Fig. 7 shows examples of the RSS measurement from experiments when omni-directional communications produce *FP* (see Fig. 7(a)) and *FN* (see Fig. 7(b)), but not for *some* directional *Pattern Pairs*. As a result, directional communications can indeed improve the accuracy of RTI systems. The poor localisation accuracy of Fig. 2(b) for omni-directional antenna is a result of a *FP* in the link quality between Nodes 2 and 5, and *FN* in the link quality near Nodes 6 and 7. We have observed many instances of such behaviour in other experiments. See Section 4.3 for the details of the statistics in the experiments.

In addition to the benefits for RTI, less radio link obstruction *FN* and *FP* can also improve the performance of other applications, e.g. people counting and speed estimation in a hallway. Specifically, two links can be deployed in the hallway to count people [15] and estimate speed [28] based on the change of the link measurements. Clearly, ESD antennas can have better performance with less radio link obstruction *FN* and *FP*.

3.2 Directional *Pattern Pair* Selection

The number of *Pattern Pairs* between two nodes can be large. Each of the nodes that we use in this paper has an ESD antenna with 6 parasitic elements. The maximum number of *Pattern Pairs* between 2 nodes is $36 \times 2 = 72$ where the 2 comes from the uplink and downlink. This means there is significant transmission overhead to make RSS measurements from all *Pattern Pairs*. This may make the dRTI

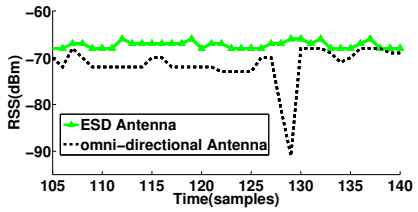

(a) example of *FP*

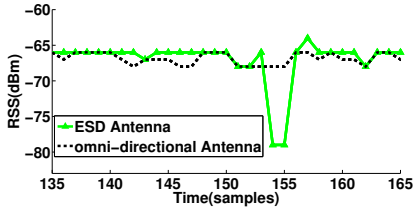

(b) example of *FN*

Figure 7: Examples of *FP* and *FN*. (a) Omni-directional communication produces a *FP* without the presence of obstructions; (b) Omni-directional communication produces a *FN* in the presence of an obstruction.

system difficult to scale to larger sizes.

Furthermore, intuitively, one may think that the *Pattern Pair* with antennas directly pointing to each other should be the "best" choice. *Is that true?* Let us look at the mRTI and vRTI for all 36 *Pattern Pairs* in Fig. 8(a) and Fig. 8(b) respectively. The answer is that the intuition is *not true*, similar to the earlier finding in wireless mesh networks [22]. For example, for vRTI in Fig. 8(b), the *Pattern Pair* with antennas directly pointing to each other is the first bar from the left which does not have the maximum RSS variance when the link is blocked by an obstruction. However, if both nodes choose Direction 6 (shown in Fig.3), this gives the first bar from the right in Fig. 8(b) which has a higher variance. The maximum variance is produced by the *Pattern Pair* between Direction 2 of the receiver and Direction 3 of the transmitter, which is the ninth bar from left in Fig. 8(b).

Similar to the earlier discovery in [3, 11], Fig. 8(a) and 8(b) also show: (1) The link qualities vary significantly between the *Pattern Pairs*; (2) Some *Pattern Pairs* have bigger change/variance than omni but some do not. This is due to the relative positions of the direction pairs and the rich multipath in the indoor environment [3]. It will pose a potential risk when the less informative *Pattern Pairs* are picked for RTI tracking, resulting in performance decrease. Therefore, we need to investigate intelligent methods to *properly* select the best directional *Pattern Pair*(s) to increase the localisation accuracy and to decrease the transmission overhead of dRTI systems. To this end, we introduce three selection methods to choose directional link *Pattern Pair*(s).

3.2.1 Location Method

This method chooses the best *Pattern Pairs* based on the physical location and orientation of the antennas. Intuitively, the *Pattern Pair* whose antennas are pointing to each other (resp. pointing in the opposite directions) should have the strongest (weakest) signal strength at the receivers, and also have higher (lower) probability to show significant RSS variances when the link between the transmitter and

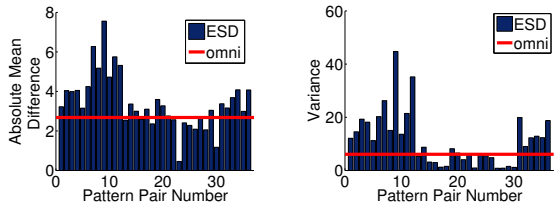

(a) mRTI (b) vRTI

Figure 8: The mRTI (a) and vRTI (b) link quality statistics for the 36 *Pattern Pairs*. The horizontal line shows the mRTI (a) and vRTI (b) for omni.

the receiver nodes is blocked by an obstruction. Though our earlier discussion shows that this intuition does not produce the best *Pattern Pair*. Nevertheless, we find from Fig. 8(a) and 8(b) that those *Pattern Pairs* that are roughly facing each other do generally give a significantly higher link quality statistics (mRTI or vRTI) than omni-directional antennas. Furthermore, this selection method *does not necessarily require an initial calibration phrase* as the other methods we will introduce, which is important for some applications such as emergency response [13].

For this method, we record the position and orientation of antennas during deployment stage. Then, according to the physical orientation of the antennas, we select $n_{transmitter}$ directions for the transmitting node N_1 and $n_{receiver}$ directions for the receive node N_2. Let N_1N_2 denote the *Link Line* connecting nodes N_1 and N_2. For the transmitter node N_1, we compute the angles (magnitude only) between the antennas on node N_1 and the *Link Line* N_1N_2, and select the directions corresponding to the $n_{transmitter}$ smallest angles. Similar method applies to choosing $n_{receiver}$ directions on N_2. In practice, we choose $n_{transmitter} = n_{receiver}$ because each node has to be transmitter and receiver. This means the number of *Pattern Pairs* selected is always a square number.

3.2.2 Fade Level Method

Wilson and Patwari define fade level in a radio link as a continuous function between the two extremes of *deep fade* and *anti-fade* in [27]. A link in deep fade will experience high variance as a person moves in a *wide* area, which may produce *FP* when the person is outside the *Link Line* of a *Pattern Pair*, e.g., outside the shadowed area in Fig. 1(b). On the other hand, an anti fade *Pattern Pair* is affected by constructive multipath interference. The link quality varies significantly less, but the radio signal attenuates significantly when a person is present in the *Link Line* of the *Pattern Pair*. Therefore, deep fade *Pattern Pair* is less informative for dRTI, and we would like to select the *Pattern Pairs* that have minimum deep fade level as in [8].

The Fade Level method collects RSS measurements of all the *Pattern Pairs* with an *empty* AoI during the calibration period $t \in [t_1, t_2]$. During the calibration, the transmitter node sends a number of (e.g., 6) packets sequentially in each direction so that receiver nodes can at least receive one packet in each antenna direction. After a fixed number of rounds (e.g., 50), the Fade Level method chooses the *Pattern Pairs* with small fade levels. Specifically, for a *Pattern Pair* between direction i of a transmitter N_1 and direc-

tion j of a receiver N_2, it computes the *normalised* RSS measurements $h_{i,j}$ during calibration period ($t \in [t_1, t_2]$) as $h_{i,j} = \sum_{t=t_1}^{t_2} r_{i,j}(t)$ where $r_{i,j}(t) = P_{tx}(i,t) - P_{rx}(i,j,t)$ where $P_{tx}(i,t)$ is the transmission power of N_1 in direction i at time t, and $P_{rx}(i,j,t)$ is the RSS measurement of receiver N_2 at direction j for the packets transmitted from N_1 in direction i at time t.

As in [8], we use $h_{i,j}$ as a measure of the fade level, and if $h_{i,j}$ is larger, the *Pattern Pair* is in a deeper fade. Therefore, the Fade Level method selects the top k *Pattern Pairs* with minimum *normalised* RSS measurements ($h_{i,j}$) from the 36 *Pattern Pairs* between N_1 to N_2.

3.2.3 Packet Reception Rate (PRR) Method

Intuitively, Packet Reception Rate (PRR) is a also good proxy for link quality because good quality links tend to have higher PRR. The PRR method also has the same calibrating period where the PRR for all *Pattern Pairs* are measured. The PRR method selects the k *Pattern Pairs* between transmitter node N_1 and receiver node N_2 that have the highest PRR during the calibration period.

3.3 Link Quality Statistics for dRTI

In Section 2.1 we present the mean and variance based link quality statistics for omni RTI. We adopt similar statistics for dRTI but they have to be modified to take into account the *Pattern Pairs*. Let F_i denote the set of selected *Pattern Pairs* for link i. Let $R_{i,j}(t)$ denote the RSS measurement at time t for the j-th *Pattern Pair* of link i. The link quality statistics for dRTI are:

- **RSS mean** Let $\bar{R}_{i,j}$ be the mean RSS over the calibration period for the j-th *Pattern Pair* in link i. The *RSS mean* statistics $y_i(t)$ for link i for dRTI is $y_i(t) = \sum_{j \in F_i} |R_{i,j}(t) - \bar{R}_{i,j}|$.
- **RSS variance** The *RSS variance* statistics for dRTI is computed over a window of v measurements. The link quality statistics $y_i(t)$ for link i for dRTI is $y_i(t) = \sum_{j \in F_i} var(R_{i,j}(t), ..., R_{i,j}(t-v+1))$

4. EVALUATION

4.1 Goals, Metrics and Methodology

The goals of our evaluation are to study: 1) whether dRTI can lead to better tracking accuracy in comparison to previous approaches based on omni-directional antennas and multi-channel RTI (cRTI); 2) the performance of Location, Fade Level and PRR *Pattern Pair* selection methods; and 3) the energy overhead of dRTI.

We use two metrics to measure the tracking accuracy. 1) *Root Mean Squared error (RMSE):* RMSE (e_{rms}) characterises the mean tracking error over the experiment and is defined as $e_{rms} = \sqrt{\frac{1}{t_d - t_c} \sum_{t=t_c}^{t_d} \hat{e}(t)^2}$ where, t_c and t_d are the experiment start time and end time respectively, and $\hat{e}(t)$ is the tracking error at time t, which is expressed as $\hat{e}(t) = \| \hat{x}(t) - x_g(t) \|$. where $\hat{x}(t)$ and $x_g(t)$ are the coordinates of the estimated location and ground truth at time t respectively. 2) *Cumulative distribution function (CDF):* CDF of an error level ℓ is the probability that the tracking error is less than or equal to ℓ. 3) *Radio link obstruction FN and FP:* The definitions of these two qualities have already been discussed in Section 3.1.4. We will present *FN* and *FP* as a percentage. *FN* (*FP*) is the ratio of the number of *FN* (*FP*) links to the total number of links.

4.1.1 Hardware and Software

We deployed a network of seven nodes with ESD antennas and one base station, which collected the RSSI measurements from all the nodes and transferred them to a PC via a serial cable for RTI and tracking. We used the nodes, which have the same hardware (TelosB and ESD antenna with six directions) and operating system (Contiki) as those used in Section 3.1.1. TelosB nodes with CC2420 transceivers operate in the 2.4 GHz ISM band and the radio channels were picked from a list {11, 15, 18, 21, 26} as in [8]. For cRTI, we used 4 channels because it showed the best tracking performance [8].

The nodes run a simple token passing protocol in a TDMA fashion similar to SPIN[3] to produce and collect radio link RSSI measurements. At a particular time, only one node transmitted packets, and the rest of the nodes received packets to measure pairwise RSS. The transmitter sent one packet per channel for cRTI and six packets per direction for dRTI in each round. The receivers *dynamically* switched antenna directions to try to collect one packet from each direction.

As introduced in Section 2.1, if the value of a voxel in the RTI image has a larger value compared to the rest, it is likely that an obstruction (a person) is located in this voxel. As in previous work [25, 26], we use the coordinate of the centre of the voxel that has the largest value in the image as the estimated location of the person since we have one person only in the experiments. We further apply a Kalman filter to produce the trajectory of the person. We use a voxel width of 0.2 m, and λ in Eq. (1) as 1.5 m. A webcam was deployed in the AoI to record ground truth for tracking.

4.1.2 Experiment Description

We conducted four experiments in our lab. Experiments 1 and 3 were conducted in a large open room for testing in a LOS environment. The black dots in Fig. 11(a) show how the seven nodes were placed in these experiments. Experiments 2 and 4 were conducted in a NLOS or "through-wall" environment. Seven nodes were placed in four adjacent rooms with four nodes in one room and one node each in the other three rooms, see Fig. 15(a). There was normal office equipment such as desk and computers in those three rooms with one node each. The walls between the rooms are made of either wood or glass.

Experiments 1 and 2 were designed to study the tracking performance of different *Pattern Pair* selection methods in LOS and NLOS environments respectively. For the purpose of comparison, we also include the tracking performance of using all 36 *Pattern Pairs*, which is termed as *All Pairs*. Experiments 3 and 4 aimed to compare the tracking accuracy of: dRTI (both mean and variance based), omni RTI (mRTI and vRTI, the transmitter sent one packet in each round.) and cRTI (both mean and variance based). Both mean and variance based RTI model have advantages. The mean based RTI model is able to detect static subjects, while the variance based RTI model does not need the calibration.

4.2 Comparing Different *Pattern Pair* Selection Methods

As discussed in Section 3.2, the *Pattern Pair* selection methods are necessary to reduce the transmission overhead, aiming to scale the larger networks and pick the informative

[3]SPIN: TinyOS code for RSS collection. SPIN: TinyOS code for RSS collection `http://span.ece.utah.edu/spin`

Pattern Pairs. Therefore, for both Experiments 1 (LOS) and 2 (NLOS), we apply the three *Pattern Pair* selection methods to compare their performance. For each experiment, both mean and variance based statistics are used. For the mean based dRTI in the LOS environment, Fig. 9(a) shows that the Fade Level and PRR methods perform similar to each other, and converge to the performance of using *All Pairs* when the number of *Pattern Pairs* is larger than 5. For the variance based dRTI, Fig. 9(b) shows that the PRR method performs best and is even better than *All Pairs*. The last result is not surprising because, as explained in Section 3.2 and from Fig. 8, we know that some *Pattern Pairs* are more informative than others, and some *Pattern Pairs* are even less informative than omni. These results also show that using all *Pattern Pairs* is not necessarily better, and judicious selection can help improve performance and reduce overhead. Fig. 10(a) also shows the similar results, all the three methods perform better than *All Pairs* when more than 1 *Pattern Pair* is chosen. For example, the Fade Level method has a nearly constant RMSE which is lower than that of *All Pairs* when the number of *Pattern Pairs* is below 30, and starts to increase after that. This is counter-intuitive because one would expect the performance becomes better when more *Pattern Pairs* are used. For the Fade Level method in Fig. 10(b), with the number of *Pattern Pairs* increasing, RMSE first decreases. After it drops to that of *All Pairs*, RMSE *increases* instead of keeping stable or decreasing. After a local peak, RMSE drops again, converging to the same level of *All Pairs*. These facts again indicates that the performance is *NOT* necessarily becoming better when more *Pattern Pairs* are picked for the tracking, as less informative *Pattern Pairs* might be included.

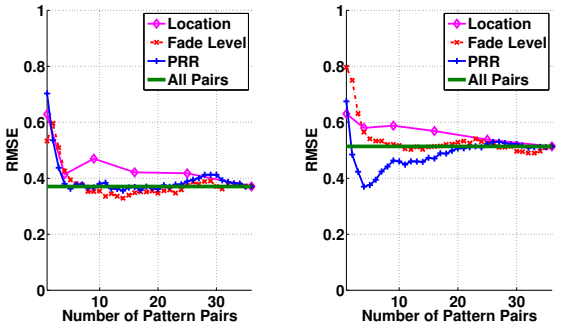

(a) mean based RTI. (b) variance based RTI

Figure 9: The tracking performance of *Pattern Pair* selection methods in the indoor LOS environment (*Experiment 1*)

In the NLOS "through-wall" environment, variance based RTI (Fig. 10(b)) significantly outperforms mean based (Fig. 10(a)) because the radio propagation environment is significantly more complicated than that of the LOS environment. Overall, Fig. 10 shows that the Fade Level method is consistently better than the other methods. This is because the Fade Level method attempts to select the *Pattern Pairs* that are *least in deep fade* to provide the most information as discussed in Section 3.2.2. Therefore, for Experiments 3 and 4, we will use the *Fade Level* method for *Pattern Pair* selection and use 9 *Pattern Pairs*.

Fig. 9 and 10 also show that the Location method performs poorly compared to the other methods. Nevertheless, it can still provide reasonably good tracking performance (approximately 0.5 metre) for both LOS (Fig. 9(a)) and NLOS (Fig. 10(b)) environments. Furthermore, the Location method does not require calibration, which makes it very useful in emergency response applications.

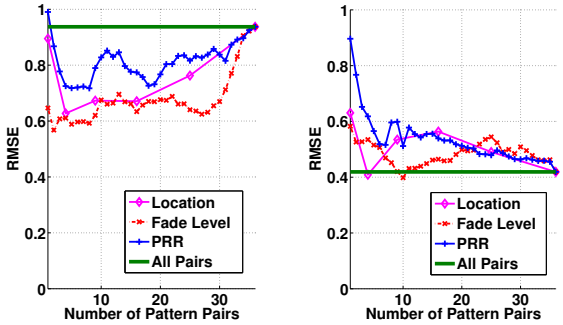

(a) mean based RTI. (b) variance based RTI

Figure 10: The tracking performance of *Pattern Pair* selection methods in the indoor NLOS "through-wall" environment (*Experiment 2*)

In summary, the Fade Level method performs best among these three methods in terms of tracking accuracy. The performance of the Location method is not as good as Fade Level, which is counter-intuitive to the directional communication in the indoor environment. This also indicates the importance of choosing the most informative *Pattern Pairs* for directional communication. Moreover, it will improve the tracking performance when picking the most informative *Pattern Pairs* instead of selecting all.

4.3 Comparing omni RTI, cRTI and dRTI

Note that in this section we use mRTI and vRTI to refer to the mean-based and variance-based *omni* RTI because these are names used in previous work. For dRTI and cRTI, it will be clear from the heading whether it is mean or variance based. As discussed earlier in Section 4.2, we will use the *Fade Level* method for *Pattern Pair* selection and use 9 *Pattern Pairs* for Experiments 3 and 4.

4.3.1 Experiment 3*: LOS environment*

Table 2: e_{rms} of mean based RTI in LOS experiment (*Experiment 3*).

method	mRTI	cRTI	dRTI
e_{rms}(m)	0.9054	0.7872	0.5221

Mean based methods: Fig. 11 shows the tracking performance of mRTI, cRTI and dRTI in the indoor LOS environment. It depicts that the trajectory estimates of dRTI is significantly closer to the ground truth compared to both mRTI and cRTI. "4m × 7m" in Fig. 11 is the size of the room. Table 2 shows the e_{rms} of mRTI, cRTI and dRTI are 0.9054 m, 0.7872 m, and 0.5221 m respectively. dRTI achieved a tracking performance improvement of approximately 42% (compared to mRTI) and approximately 34% (compared to cRTI). The CDFs for different mean based RTI methods are presented in Fig. 12. The results show that the 90th percentile tracking errors for mRTI, cRTI, and dRTI were approximately 1.5 m, 1.2 m and 0.7 m respectively. In this metric, dRTI achieved performance improvements of approximately 53% (compared to mRTI) and 42% (compared

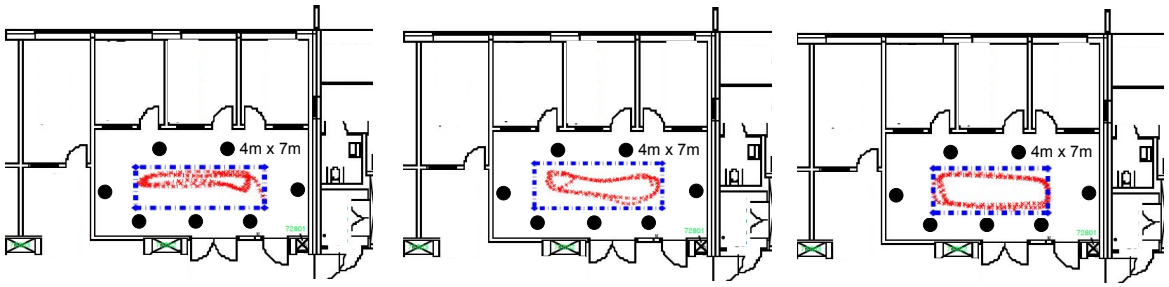

(a) mRTI (b) cRTI (RSS mean) (c) dRTI (RSS mean)

Figure 11: The tracking performance of mean based RTI in the LOS experiment of omni RTI, cRTI, and dRTI. The red lines are the trajectory estimates of the different methods, and the dotted blue lines are the ground truth (*Experiment 3*).

to cRTI) respectively.

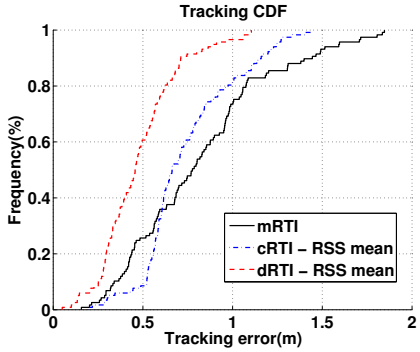

Figure 12: The CDFs of mean based RTI methods (*Experiment 3*).

Variance based methods: The tracking performance shows similar results as Fig. 11. We omit this tracking performance figure for the benefit of space.[4] Table 3 shows, the e_{rms} of vRTI, cRTI and dRTI are 0.7196 m, 0.5565 m, and 0.4340 m respectively. dRTI achieved a tracking performance improvement of approximately 40% (compared to vRTI) and approximately 22% (compared to cRTI). The CDFs for different variance based RTI methods are presented in Fig. 13. The 90th percentile tracking errors for vRTI, cRTI, and dRTI were approximately 1.1 m, 0.75 m and 0.7 m respectively. In this metric, dRTI achieved performance improvements of approximately 36% (compared to vRTI) and 7% (compared to cRTI) respectively.

Table 3: e_{rms} of variance based RTI in LOS experiment (*Experiment 3*).

method	vRTI	cRTI	dRTI
e_{rms}(m)	0.7196	0.5565	0.4340

Radio Obstruction *FN* and *FP*: Fig. 14 shows the statistics of radio link obstruction *FN* and *FP*. The state of radio channels can be divided into two classes, i.e. non-fading and shadowing. Non-fading is the state when the LOS is clear, while the shadowing means the LOS is blocked. We use the conditions in Eq. (1) to decide the state of the channel. Fig. 14(a) and Fig. 14(b) show the statistics of radio link obstruction *FN* and *FP*, when channels are divided into two states. The figures compares three classes

[4] All the omitted figures will be made public in a technical report.

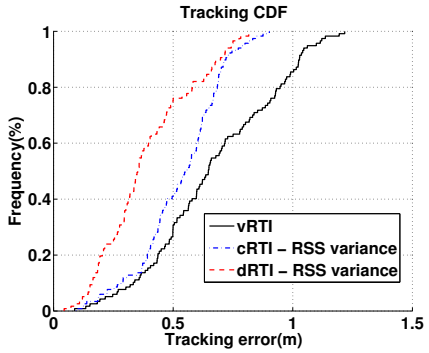

Figure 13: The CDFs of variance based RTI methods (*Experiment 3*).

of methods: m/vRTI,cRTI and dRTI. For each method, we vary the threshold used to determine whether a link is *FP* and *FN*. We know from the standard theory on statistical hypothesis testing that there is a trade-off between *FP* and *FN*. This trade-off is clearly visible in the figure. We know that if a method can achieve lower *FP* and *FN*, then it is a better method. It is clear from Fig. 14 that dRTI has the lowest *FP* and *FN* compared with the other two methods. These statistics support the hypotheses in Section 3.1.4 and provide an insight on why dRTI perform better than omni-directional RTI and cRTI as shown in Table 2 and Table 3.

4.3.2 Experiment 4*: NLOS "Through-wall" environment*

Table 4: e_{rms} of mean based RTI in NLOS experiment (*Experiment 4*).

method	mRTI	cRTI	dRTI
e_{rms}(m)	1.4922	0.8580	0.7506

Mean based methods: Compared to the performance in the LOS environment in Section 4.3.1, the NLOS "through-wall" environment is significantly more challenging for RTI, and the tracking errors are significantly higher for all RTI methods. However, Fig. 15 shows the tracking performance of mRTI, cRTI and dRTI in a NLOS "through-wall" environment. It demonstrates that the trajectory estimates of dRTI is significantly closer to the ground truth compared to both mRTI and cRTI. Table 4 shows, the e_{rms} of mRTI, cRTI and dRTI are 1.4922 m, 0.8580 m, and 0.7506 m respectively. dRTI achieves a tracking performance improvement of approximately 50% (compared to mRTI) and ap-

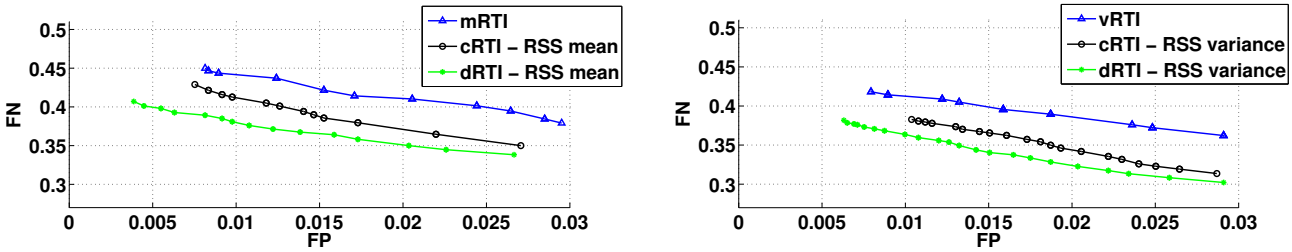

(a) mean based RTI. (b) variance based RTI.

Figure 14: The statistics for Radio Link Obstruction *FN* and *FP* in the indoor LOS environment (*Experiment 3*)

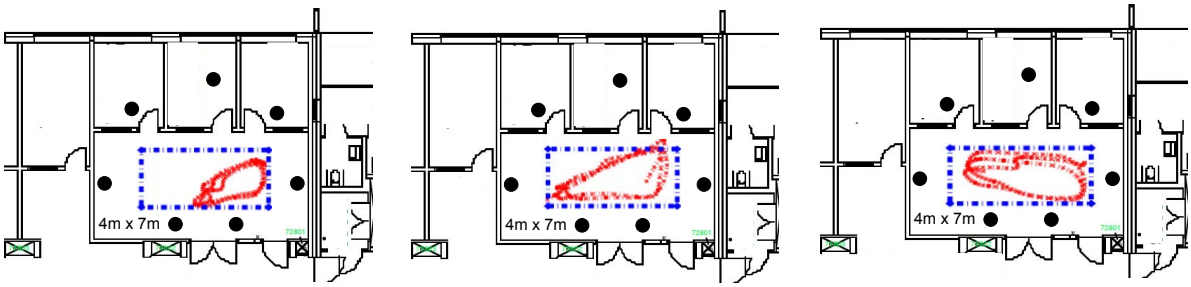

(a) mRTI (b) cRTI (RSS mean) (c) dRTI (RSS mean)

Figure 15: The tracking performance of mean based RTI in the NLOS "through-wall" experiment of RTI, cRTI, and dRTI. The red lines are the trajectory estimates of the different methods, and the dotted blue lines are the ground truth (*Experiment 4*).

proximately 12% (compared to cRTI). The CDFs for different mean based RTI methods were showed in Fig. 16. The 90th percentile tracking errors for mRTI, cRTI, and dRTI were approximately 2.4 m, 1.3 m and 1.2 m respectively. In this metric, dRTI achieves performance improvements of approximately 50% (compared to mRTI) and 8% (compared to cRTI) respectively.

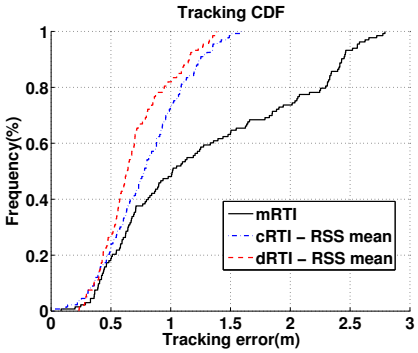

Figure 16: The CDFs of mean based RTI methods (*Experiment 4*).

Table 5: e_{rms} of variance based RTI in NLOS experiment (*Experiment 4*).

method	vRTI	cRTI	dRTI
e_{rms}(m)	1.0432	0.8574	0.6734

Variance based methods: Previous work showed that variance based RTI methods significantly outperformed mean based RTI methods in NLOS "through-wall" environments [26]. Our results in Tables 4 and 5 also confirm this finding. As for the tracking performance, it demonstrates the similar results shown in Fig. 15. We omit this tracking performance figure for the benefit of space. Table 5 also shows, the e_{rms} of vRTI, cRTI and dRTI are 1.0432 m, 0.8574 m, and 0.6734 m respectively. dRTI achieves a tracking performance improvement of approximately 35% (compared to vRTI) and approximately 21% (compared to cRTI). The CDFs for different variance based RTI methods are presented in Fig. 17. The 90th percent of tracking errors for vRTI, cRTI, and dRTI were approximately 1.7 m, 1.2 m and 1 m respectively. In this metric, dRTI achieves performance improvements of approximately 41% (compared to vRTI) and 17% (compared to cRTI) respectively.

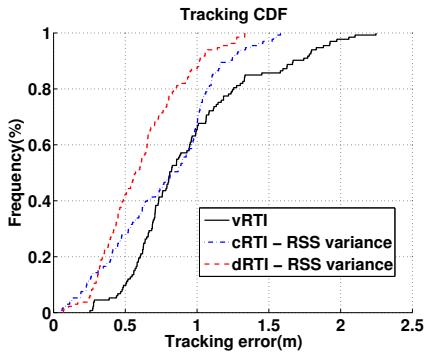

Figure 17: The CDFs of variance based RTI methods (*Experiment 4*).

Radio Obstruction *FN* and *FP*:
The statistics of radio obstruction *FN* and *FP* in this experiment show similar results shown in Fig. 14. We omit

the figures for the benefit of space.

4.4 Energy Cost

We measured the energy consumption of our dRTI system by connecting a node to a 10 ohm resistor in series of the power supply and measured the voltage across the resistor by an oscilloscope. For small beacon packets whose payload length is 5 bytes, consisting of node ID (2 bytes), transmit direction (1 byte), and sequence number (2 bytes), the energy consumption was approximately 55 μJ. For large packets for transferring RSS measurements to the base station with payload length of 62 bytes, the energy consumption was approximately 179 μJ. The transmission time for the 5-byte beacon packets and 62-byte large packets were approximately 0.72 ms and 2.85 ms respectively. The receiver consumes 60 mW when the radio is on. The energy consumption was measured when the transmit power is set to the maximum value of 31. The nodes are powered by two AA 2400 mAh batteries in serial. When the radio duty cycle is 100%, our dRTI system will run approximately 117 hours. There is a clear need for through-wall surveillance in emergency situations to help save lives during a building fire or a hostage situation [13], but few such situations will last more than a day. There is little incentive to increase lifetime further, as we are not developing the technology to be used for long-term through-wall surveillance of a subject in their home or place of work.

5. RELATED WORK

Ultra-wideband (UWB) impulse radar devices have been studied for through-wall imaging. They transmit wideband impulses, and estimate the distance to a scatterer by measuring the time delay of the echo. UWB impulse radar typically performs well at short range. However, the accuracy decreases at long range because of limited transmit power and d^4 scattering losses [25].

Recently, many RSS-based device-free localization methods have been proposed. Youssef et al. used the variance or change in RSS to detect a person crossing a link [32]. Patwari and Agrawal proposed to use tomography to estimate an image of the AoI based on the signal obstruction of many radio links (mRTI) [18], which they called RTI. However, their following work in [26] showed that mRTI was ineffective in the "through-wall" setting because the radio signal statistics behaved unexpectedly. Their experiment showed the RSS measurements may decrease, keep stable or even increase when a link was blocked by an obstruction. Therefore, instead of using mRTI, they proposed to use the variance-based RTI (vRTI) in [26]. Later, Kaltiokallio et al. proposed to use multiple independent channels to increase the performance of RTI (cRTI) in [8]. In cRTI, performance improves with the number of channels measured. Channel diversity requires more bandwidth compared to single-channel RTI, and is limited by the number of "clean" or interference-free radio channels. *With ubiquitous use of wireless technologies such as WiFi, it becomes more and more difficult to dedicate bandwidth, particularly in ISM bands, for RTI systems.* To this end, the proposed dRTI requires only one channel, the same as the traditional single-channel RTI. [27, 16] developed signal strength models for indoor localisation, while our paper focuses on studying the ESD antennas' performance on RTI. Bocca et al. proposed to manually rotate nodes to calibrate their positions and orientations in order to improve the RTI performance [5], while the nodes in our method can conduct the calibration automatically and attempt to select the best *Pattern Pairs* for RTI. ESD antennas can also help reduce the instances of *FP* and *FN*. Furthermore, dRTI could apply the proposed methods in [5] to calibrate the positions of ESD antennas, but this is beyond the scope of this paper.

RSS fingerprint-based methods for device free indoor localisation and tracking have been investigated in [29, 30, 31]. Fingerprint-based methods do not require the sensor coordinates to be known, and they adaptively learn the multipath characteristics of an environment. This paper shows that use of directional antennas in a wireless network increases the effect that a person has on the RSS. Further, having a diversity of directional patterns effectively increase the dimension of the RSS fingerprint. Both effects could be applied to improve the accuracy of RSS fingerprint-based methods as well, although the focus in this paper has been on RTI. Some applications also use Channel State Information to fingerprint location [21] and activities [24, 23], but they need extra effort to modify firmware.

Fingerprint-based methods require training periods in which a person is required to walk in each voxel in the AoI while the systems collect RSS fingerprints, as well as an empty-room training period. In contrast, mRTI requires only the empty-room training period, and vRTI requires no training period. vRTI is advantageous since training is not possible in emergency response applications, however, vRTI is cannot detect static objects in the AoI. Edelstein and Rabbat proposed a method to identify the background (no person obstructing) RSS from a radio link that has periods of obstruction and no obstruction [6]. This work is complementary to the approaches in [6, 33] and one could add directionality to improve the performance of [6, 33].

Adib and Katabi recently proposed WiVi to count the number of people "through-wall" and recognise simple gestures based on WiFi signals in [2]. WiVi can count the number of people and estimate their relative velocity. Pu et al. developed WiSee, which demonstrated high classification accuracy among a set of nine gestures, using Doppler shift measurements and machine learning [20]. Kellogg et al. also proposed AllSee for gesture recognition, which applied existing wireless signals and battery-free devices to save energy [10]. In contrast, our paper focuses on tracking the absolute positions of people indoors. Adib et al. developed WiTrack using the Frequency-Modulated Carrier Waves (FMCW) technology to track the persons' motion, and this was used for 3D tracking and achieved good performance [1]. However, WiTrack needed to sweep a bandwidth of 1.6 GHz for high accuracy, while our dRTI only uses one channel with 5 MHz bandwidth in the 2.4 GHz band. To compare with dRTI, we only consider the horizontal dimension, WiTrack's median location error is 13 cm in the LOS experiment and 16 cm in the NLOS experiment. As the resolution is inversely proportional to the total sweeping bandwidth according to Eq. (3) in [1], the resolution would be 41.6 m and 51.2 m separately if only a 5 MHz bandwidth is available for WiTrack. The methods proposed and evaluated in this paper are complementary to techniques proposed in [1, 2, 20]. If ESD antennas can improve RTI, they presumably could improve results for Doppler or time-delay based methods for localisation and gesture recognition as well, by reducing susceptibility to multipath and focussing more energy on the person being tracked.

6. CONCLUSIONS

In this paper, we investigate how directional antennas can be used to improve localisation accuracy of RTI. We implement dRTI and show that obstructions have a greater impact on the link quality of directional links. We also show dRTI has less *FN* and *FP* of radio link obstruction measurements. These in turn significantly improve the localisation accuracy of dRTI. Since the number of antenna direction pairs between two dRTI nodes can be large (e.g., 36 in our dRTI system), we further propose methods to effectively select informative antenna direction pairs to reduce communication and energy overhead. We evaluate the proposed dRTI system in different indoor environments. Our extensive experiments show that dRTI significantly outperforms omni-directional RTI and multi-channel RTI in both line-of-sight (LOS) and non-LOS "through-wall" environments.

Acknowledgements. We thank our shepherd, Dr. Anthony Rowe, the anonymous reviewers and our internal reviewer, Dr. Brano Kusy for their helpful feedbacks on earlier versions of this paper.

7. REFERENCES

[1] F. Adib, Z. Kabelac, D. Katabi, and R. C. Miller. 3D tracking via body radio reflections. In *NSDI '14*, Seattle, WA, 2014.

[2] F. Adib and D. Katabi. See through walls with WiFi! In *SIGCOMM '13*, pages 75–86, New York, NY, USA, 2013. ACM.

[3] A. Amiri Sani, L. Zhong, and A. Sabharwal. Directional antenna diversity for mobile devices: Characterizations and solutions. In *MobiCom '10*, pages 221–232, New York, NY, USA, 2010. ACM.

[4] M. Bocca, O. Kaltiokallio, and N. Patwari. Radio tomographic imaging for ambient assisted living. In *Evaluating AAL Systems Through Competitive Benchmarking*, pages 108–130. Springer, 2013.

[5] M. Bocca, A. Luong, N. Patwari, and T. Schmid. Dial it in: Rotating RF sensors to enhance radio tomography. *IEEE SECON 2104*, July, 2013.

[6] A. Edelstein and M. Rabbat. Background subtraction for online calibration of baseline rss in rf sensing networks. *IEEE TMC*, 12(12):2386–2398, 2013.

[7] G. Giorgetti, A. Cidronali, S. Gupta, and G. Manes. Exploiting low-cost directional antennas in 2.4 GHz ieee 802.15.4 wireless sensor networks. In *EuMW'07*, 2007.

[8] O. Kaltiokallio, M. Bocca, and N. Patwari. Enhancing the accuracy of radio tomographic imaging using channel diversity. In *MASS*, pages 254–262. IEEE Computer Society, 2012.

[9] O. Kaltiokallio, M. Bocca, and N. Patwari. Follow @grandma: long-term device-free localization for residential monitoring. In *IEEE SenseApp 2012*, pages 984–991, Clearwater, Florida, USA, 2012. IEEE.

[10] B. Kellogg, V. Talla, and S. Gollakota. Bringing gesture recognition to all devices. In *NSDI 14*, Seattle, WA, 2014. USENIX.

[11] S. Lakshmanan, K. Sundaresan, S. Rangarajan, and R. Sivakumar. The myth of spatial reuse with directional antennas in indoor wireless networks. In *Passive and Active Measurement*, volume 6032 of *Lecture Notes in Computer Science*, pages 51–60. Springer Berlin Heidelberg, 2010.

[12] X. Liu, A. Sheth, M. Kaminsky, K. Papagiannaki, S. Seshan, and P. Steenkiste. DIRC: Increasing indoor wireless capacity using directional antennas. In *SIGCOMM '09*, pages 171–182, New York, NY, USA, 2009. ACM.

[13] D. Maas, J. Wilson, and N. Patwari. Toward a rapidly deployable RTI system for tactical operations. In *SenseApp 2013*, 2013.

[14] L. Mottola, T. Voigt, and G. P. Picco. Electronically-switched directional antennas for wireless sensor networks: A full-stack evaluation. In *SECON '13*, pages 176–184, 2013.

[15] M. Nakatsuka, H. Iwatani, and J. Katto. A study on passive crowd density estimation using wireless sensors. In *ICMU 2008*. Citeseer, 2008.

[16] S. Nannuru, Y. Li, Y. Zeng, M. Coates, and B. Yang. Radio-frequency tomography for passive indoor multitarget tracking. *IEEE TMC*, 12(12):2322–2333, Dec 2013.

[17] M. Nilsson. Directional antennas for wireless sensor networks. In *Adhoc'09*, 2009.

[18] N. Patwari and P. Agrawal. Effects of correlated shadowing: Connectivity, localization, and RF tomography. In *IPSN '08*, pages 82–93, 2008.

[19] N. Patwari and J. Wilson. Spatial models for human motion-induced signal strength variance on static links. *IEEE TIFS*, 6(3):791–802, Sept 2011.

[20] Q. Pu, S. Gupta, S. Gollakota, and S. Patel. Whole-home gesture recognition using wireless signals. In *MobiCom 2013*, pages 27–38, Sept. 2013.

[21] S. Sen, B. Radunovic, R. R. Choudhury, and T. Minka. You are facing the Mona Lisa: spot localization using PHY layer information. In *MobiSys 2012*, pages 183–196. ACM, 2012.

[22] A. P. Subramanian, H. Lundgren, and T. Salonidis. Experimental characterization of sectorized antennas in dense 802.11 wireless mesh networks. In *MobiHoc '09*, pages 259–268. ACM, 2009.

[23] Y. Wang, J. Liu, Y. Chen, M. Gruteser, J. Yang, and H. Liu. E-eyes: device-free location-oriented activity identification using fine-grained wifi signatures. In *MobiCom 2014*, pages 617–628. ACM, 2014.

[24] B. Wei, W. Hu, M. Yang, Chou, and C. Tung. Radio-based device-free activity recognition with radio frequency interference. In *IPSN '15*, Seattle, WA, USA, 2015. ACM.

[25] J. Wilson and N. Patwari. Radio tomographic imaging with wireless networks. *IEEE TMC*, 9(5):621–632, 2010.

[26] J. Wilson and N. Patwari. See-through walls: Motion tracking using variance-based radio tomography networks. *IEEE TMC*, 10(5):612–621, 2011.

[27] J. Wilson and N. Patwari. A fade-level skew-laplace signal strength model for device-free localization with wireless networks. *IEEE TMC*, 11(6):947–958, 2012.

[28] K. Woyach, D. Puccinelli, and M. Haenggi. Sensorless sensing in wireless networks: Implementation and measurements. In *WiOpt 2006*, pages 1–8. IEEE, 2006.

[29] C. Xu, B. Firner, R. S. Moore, Y. Zhang, W. Trappe, R. Howard, F. Zhang, and N. An. SCPL: Indoor device-free multi-subject counting and localization using radio signal strength. In *IPSN '13*, pages 79–90, New York, NY, USA. ACM.

[30] C. Xu, B. Firner, Y. Zhang, R. Howard, J. Li, and X. Lin. Improving rf-based device-free passive localization in cluttered indoor environments through probabilistic classification methods. In *IPSN '12*, pages 209–220, New York, NY, USA. ACM.

[31] C. Xu, M. Gao, B. Firner, Y. Zhang, R. Howard, and J. Li. Towards robust device-free passive localization through automatic camera-assisted recalibration. In *ACM SenSys*, 2012.

[32] M. Youssef, M. Mah, and A. Agrawala. Challenges: device-free passive localization for wireless environments. In *MobiCom '07*, pages 222–229, New York, NY, USA, 2007. ACM.

[33] Y. Zhao, N. Patwari, J. M. Phillips, and S. Venkatasubramanian. Radio tomographic imaging and tracking of stationary and moving people via kernel distance. In *IPSN '13*, pages 229–240, New York, NY, USA. ACM.